SIGNAL MODEL AND MOVING TARGET DETECTION BASED ON MIMO SYNTHETIC APERTURE RADAR

W. Zhou[*], J. T. Wang, H. W. Chen, and X. Li

School of Electronic Science and Engineering, National University of Defense Technology, Changsha 410073, China

Abstract—Recent years, a new SAR concept based on Multi-Input Multi-Output (MIMO) configuration has demonstrated the potential advantages to simultaneously improve the performance of Synthetic Aperture Radar (SAR) imaging and ground moving target detection by utilizing multiple antennas both at transmission and reception. However, the precise signal model, as well as the effect of ground moving target in image domain and the approaches for moving target indication based on MIMO SAR system are rarely investigated. Our paper has three main contributions. Firstly, we present a detailed signal model for stationary scene and moving target based on a colocated MIMO SAR configuration, and analyze the motion effect of the moving target. Secondly, we provide an algorithm of phase compensation to combine the multiple virtual channel data in order to enhance the image quality. Thirdly, an adaptive optimal approach is applied for clutter suppression, then the velocity of the moving target is estimated via Delay-and-Sum (DAS) beamforming approach. Finally, several numerical experiments are provided to illustrate the derivation and analysis in this paper.

1. INTRODUCTION

Recently, a great of interest has been attracted by a conception of Multi-Input Multi-Output (MIMO) radar [1–7], where multiple antennas are used both at transmission and reception to exploit spatial and waveform diversity gain simultaneously. Primary studies have demonstrated the potential advantages to simultaneously improve the performance of wide swath Synthetic Aperture Radar (SAR) imaging and ground moving target detection by utilizing multiple antennas both at transmission and reception [8–14].

The SAR concept based on MIMO array is first proposed by Ender [15], which is a natural extension of multi-channel SAR except for employing multiple transmit antennas and orthogonal waveform sets. Such an extension has been suggested for a variety of applications. A new notion of digital radar system combining waveform encoding on transmission with digital beamforming on reception is presented in [8], which is able to resolve the hitherto contradicting requirements for high resolution and wide coverage. The performance improvement for range resolution of SAR by multiple transmit and receive platforms with adequate cross-track displacement is investigated in [16], and the novel system concept for interferometric SAR based on MIMO configuration is proposed in [17]. The use of multiple transmit antennas to improve the performance of the Velocity Synthetic Aperture Radar (VSAR) system is investigated in [18, 19]. Furthermore, some types of experimental systems have been developed. For instance, the experimental X-band radar called PAMIR can be operated as MIMO mode [20]. The imaging MIMO radar MIRA-CLEX, which operates at X-band with 16 transmit and 14 receive elements, can generate at most 224 virtual phase centers through multiple-input and multiple-output signal processing [21]. An airborne S-band MIMO radar testbed is developed by Lincoln Laboratory with up to 6 independent transmit channels and 8 independent receive channels, and the GMTI experiments have demonstrated the potential for the enhanced GMTI performance using MIMO techniques [22].

We focus on the stationary target imaging and ground moving target detection based on MIMO SAR configuration in this paper. The rest of the paper is organized as follows. In Section 2, we derive the signal models for both stationary and moving targets based on the MIMO SAR system with colocated antennas. The scheme for imaging processing to combine the multi-channel complex images is proposed in Section 3. In Section 4, an optimal adaptive algorithms for clutter suppression and the classical Delay-and-Sum (DAS) algorithm for velocity estimation is presented. In Section 5, we design several simulated experiments to illustrate the derivation and analysis in this paper, and a conclusion is given in Section 6.

2. SIGNAL MODEL BASED ON MIMO SAR

2.1. Geometry of MIMO SAR

A 3-dimensional (3-D) geometry of MIMO SAR system equipped with colocated transmit/receive antennas is shown in Fig. 1. The platform moves with a velocity v_p and height h along x axis. There are M transmit antennas and N receive antennas equally placed along with
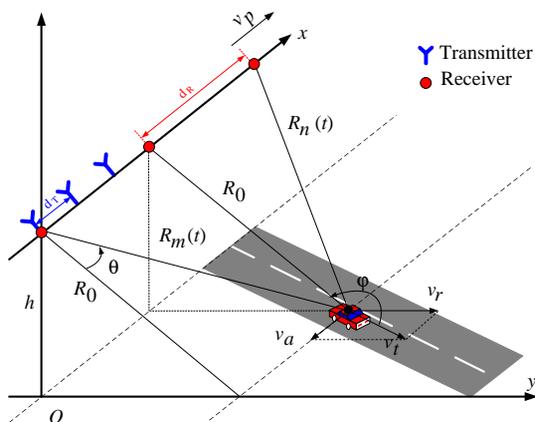
Figure 1. Geometry of MIMO SAR.

the azimuth direction. Without loss of generality, we assume that the first transmitter and the first receiver are both located at $x = 0$, and the rest of the antennas are equally spaced along x-axis with the inter spacings of d_T and d_R, respectively. The coordinate of the mth transmit antenna can therefore be denoted by $x_m^t = (m-1) \cdot d_T$, $m = 1, 2, \ldots, M$, as well as the coordinate of the nth receive antenna can be written by $x_n^r = (n-1) \cdot d_R$, $n = 1, 2, \ldots, N$.

In order to separate the multiple transmit signals at reception, a set of orthogonal waveforms with perfect auto- and cross-correlation properties should be transmitted. The mth transmit waveform $s_m(t)$ is given by

$$s_m\left(t, \hat{t}\right) = rect\left(\frac{\hat{t}}{T_p}\right) u_m\left(\hat{t}\right) \exp\left(j2\pi f_c t\right), \tag{1}$$

where the symbols are explained as follows: $rect(\hat{t}/T_p)$ is the rectangular window function, $u_m\left(\hat{t}\right)$ denotes the complex envelop, f_c is the carrier frequency, T_p is the pulse width, $\hat{t}$ and t represent the fast time and the absolute time, respectively. The number of pulses integrated during the synthetic aperture time is denoted by L_s, thus $t = \hat{t} + l_s T$, $l_s = 0, 1, \ldots, L_s - 1$, with T representing the pulse reception interval.

Due to the hypothesis of orthogonality, the set of waveforms satisfies

$$\int u_m\left(\hat{t}\right) u_n^*\left(\hat{t} + \tau\right) d\hat{t} = \begin{cases} 1, & m = n, \\ 0, & m \neq n. \end{cases} \tag{2}$$

where τ is the arbitrary time lag.

The special mode of multiple transmit and multiple receive antennas provides extra degree of freedom (DOF) for waveform design. The waveforms can vary not only on pulse-by-pulse basis, but also on antenna-by-antenna. Therefore, how to design a set of waveforms to maximize the system performance of MIMO radar has become a critical issue [23–25], although this is beyond our topic in this paper.

2.2. Signal Model for Stationary Target

We assume that an ideal stationary point target P is located at (x, y) with the complex scatter coefficient $\sigma_c(x, y)$. The one-way range histories of the target from P to the phase center of the mth transmit antenna and the nth receive antenna are denoted by [13]

$$R_m^t(t) = \sqrt{(x - x_m^t - v_p t)^2 + y^2 + h^2} \approx R_0 + \frac{(x - x_m^t - v_p t)^2}{2R_0} \quad (3)$$

$$R_n^r(t) = \sqrt{(x - x_n^r - v_p t)^2 + y^2 + h^2} \approx R_0 + \frac{(x - x_n^r - v_p t)^2}{2R_0} \quad (4)$$

respectively, where $R_0 = \sqrt{y^2 + h^2}$ is the minimum slant range.

The complete measured signal received by the nth receive antenna is a superposition of echoes back from the the scene illuminated by all the transmit signals, thus,

$$
\begin{aligned}
y_n(t, \hat{t}) &= \sum_{m=1}^{M} \iint_{x,y \in \Omega} \sigma_c(x, y) s_m\left(t - \frac{R_{mn}(t)}{c}\right) dx dy \\
&= \sum_{m=1}^{M} \iint_{x,y \in \Omega} \sigma_c(x, y) w_r\left(\hat{t} - \frac{R_{mn}(t)}{c}\right) w_a(t) \\
&\quad \cdot u_m\left(\hat{t} - \frac{R_{mn}(t)}{c}\right) \exp\left(-j\frac{2\pi}{\lambda} R_{mn}(t)\right) dx dy \quad (5)
\end{aligned}
$$

where $R_{mn}(t) = R_m^t(t) + R_n^r(t)$ is the round-trip range history from the mth transmit phase center to the target, and back to the nth receive phase center; $w_r(\hat{t})$ and $w_a(t)$ denote the window function in range and azimuth, respectively; Ω denotes the image area on the ground.

After demodulation, a bank of match filters are applied at each receiver to separate the multiple transmit waveforms. Due to hypothesis of perfect orthogonality of the waveforms, complete separation can be achieved here. The signals of the mnth transmit-

receive pair therefore can be expressed as

$$y_{mn}(\hat{t}, t) \approx \iint\limits_{x,y\in\Omega} \sigma_c(x, y) A_r \operatorname{sinc}\left(B_r\left[\hat{t} - \frac{R_{mn}(t)}{c}\right]\right)$$

$$\cdot \exp\left(-j\frac{2\pi}{\lambda}\left[2R_0 + \frac{(x - x_m^t)^2 + (x - x_n^r)^2}{2R_0}\right]\right)$$

$$\cdot w_a(t) \exp\left(j2\pi\frac{2v_p(x - x_e)}{\lambda R_0}t + j\pi\frac{-2v_p^2}{\lambda R_0}t^2\right) dxdy, \quad (6)$$

where A_r is the pulse compression gain in range, B_r is the bandwidth of each transmit waveform, and $\operatorname{sinc}(x) = \sin(\pi x)/(\pi x)$.

The equivalent virtual phase center resulted from mth transmit antenna and nth receive antenna is denoted by $x_e(m, n) = (x_m^t + x_n^r)/2$. When the antennas are colocated, there will be an approximation $(x - x_m^t)^2 + (x - x_n^r)^2 \approx 2(x - x_e)^2$. Therefore, the first exponential term in (6) is approximate to $\exp(-j2\pi(x - x_e)^2/(\lambda R_0))$, only need to compensate the constant phase term $\exp(j2\pi(x_m^t - x_n^r)^2/(4\lambda R_0))$.

Then (6) can be rewritten by

$$y_{mn}(\hat{t}, t) = \iint\limits_{x,y\in\Omega} \sigma_c(x, y) A_r \operatorname{sinc}\left(B_r\left[\hat{t} - \frac{R_{mn}(t)}{c}\right]\right)$$

$$\cdot w_a(t) \exp\left(-j\frac{2\pi}{\lambda}\left[2R_0 + \frac{(x - x_e)^2}{R_0}\right]\right)$$

$$\cdot \exp\left(j2\pi f_{dc,mn}t + j\pi f_{dr,mn}t^2\right) dxdy, \quad (7)$$

where the terms $f_{dc,mn} = 2v_p(x - x_e)/(\lambda R_0)$ and $f_{dr,mn} = -2v_p^2/(\lambda R_0)$ denote the Doppler centroid and modulation frequency of the azimuth signals, respectively.

In the case of a single colocated transmitter and receiver, the expression in (7) will reduces to a general signal mode of conventional SAR system [26, 30].

It clearly shows that there is an azimuth Doppler shift of the signal from the mnth transmit-receive pair compared to the conventional single SAR system because of the displacement of multiple virtual phase centers.

2.3. Signal Model for Moving Target

Similarly with the derivation of signal model for stationary target, we assume there are N_T discrete scatterers located at a resolution cell with

complex coefficient $\sigma_{T,i}$, the azimuth angle denoted by θ, and the angle between the moving direction and light of sight is φ. The along-track and cross-track velocity are denoted by v_a and v_r, respectively. Since the velocity of ground moving target is ordinarily slow, it is reasonable to suppose the velocity vector is kept constant during the synthetic aperture interval.

Based on the assumption aforementioned, the range history of the moving target is denoted by

$$R_m^t\left(t\right) \approx R_0 + v_r t + \frac{\left(x - x_m^t - v_e t\right)^2}{2R_0}, \tag{8}$$

$$R_n^r\left(t\right) \approx R_0 + v_r t + \frac{\left(x - x_n^r - v_e t\right)^2}{2R_0}, \tag{9}$$

respectively. The symbol $v_e = v_p - v_a$ denotes the relative velocity of the platform. For ground slow moving target, there is $v_a \ll v_p$, especially for spaceborne SAR system, then $v_e \approx v_p$.

The signals received by the nth receive antenna from multiple moving targets can be written as

$$y_n\left(t, \hat{t}\right) = \sum_{m=1}^{M}\sum_{i=1}^{N_T} \sigma_{T,i}\left(x, y\right) w_r\left(\hat{t} - \frac{R_{mn}\left(t\right)}{c}\right) w_a\left(t\right)$$

$$\cdot u_m\left(\hat{t} - \frac{R_{mn}\left(t\right)}{c}\right) \exp\left(-j\frac{2\pi}{\lambda}R_{mn}\left(t\right)\right). \tag{10}$$

Just as the processing in Section 2.2, a bank of match filters are applied at each receiver. The signals of the mnth transmit-receive pair can therefore be expressed as

$$y_{mn}(\hat{t}, t) \approx \int y_n(\hat{t}, t) \cdot s_m{}^*(\hat{t}, t) d\hat{t}$$

$$= \sum_{i=1}^{N_T} \sigma_{T,i}\left(x, y\right) A_r \operatorname{sinc}\left(B_r\left[\hat{t} - \frac{R_{mn}(t)}{c}\right]\right) \cdot w_a\left(t\right)$$

$$\cdot \exp\left(-j\frac{2\pi}{\lambda}\left[2R_0 + \frac{(x - x_e)^2}{R_0}\right]\right) \exp\left(j2\pi\frac{-2v_r}{\lambda}t\right)$$

$$\cdot \exp\left(j2\pi\frac{2v_e\left(x - x_e\right)}{\lambda R_0}t\right) \exp\left(j\pi\frac{-2v_e^2}{\lambda R_0}t^2\right). \tag{11}$$

Relatively to the received signals of stationary target in (7), there is an extra azimuth Doppler shift due to the cross-track velocity of the moving target, which will result in the azimuth displacement in images. In addition, the residual Doppler rate will result in the image

defocused. Fortunately, the variation of the Doppler rate is normally small, especially for spaceborne platform with extreme high velocity, then the main energy of the moving target will still be assumed to distribute within a single resolution cell.

3. IMAGING PROCESSING

For stationary target, the reference signal for azimuth compression is constructed by

$$s_{ref}\left(t\right) = w_{ra}\left(t\right)\exp\left(j2\pi\left[f_{dc}t + \frac{1}{2}\beta t^2\right]\right),\qquad(12)$$

where $f_{dc} = 2v_p x/\lambda R_0$ denotes the centroid of Doppler frequency; $\beta = -2v_p^2/\lambda R_0$ is the Doppler modulation rate in azimuth; $w_{ra}(t)$ is the reference window function in azimuth.

According to the principle of stationary phase [26], the reference signal for stripmap SAR mode in frequency domain can be written as

$$S_{ref}\left(f_a\right) = W_{ra}\left(f_a\right)\exp\left(-j\pi\frac{\lambda R_0 f_a^2}{2v_p^2}\right).\qquad(13)$$

3.1. Imaging Processing for Stationary Target

The signal of the mnth transmit-receive pair in range-Doppler domain is

$$y_{mn}\left(\hat{t}, f_a\right) = \iint\limits_{x,y\in\Omega}\sigma_c\left(x,y\right) A_r \operatorname{sinc}\left(B_r\left[\hat{t} - \frac{R_{mn}(t)}{c}\right]\right)$$

$$\cdot W_a\left(f_a\right)\exp\left(-j\frac{2\pi}{\lambda}\left[2R_0 + \frac{(x-x_e)^2}{R_0}\right]\right)$$

$$\cdot\exp\left\{-j\pi\frac{\lambda R_0}{2v_p^2}(f_a - f_{dc,mn})^2\right\}dxdy.\qquad(14)$$

After compensation of range migration, pulse compression is implemented in azimuth direction, then the stationary scene image is denoted by

$$y_{mn}\left(\hat{t},t\right) = \iint\limits_{x,y\in\Omega}\sigma_c\left(x,y\right) A_r A_a\cdot\operatorname{sinc}\left(B_r\left[\hat{t} - \frac{R_{mn}(t)}{c}\right]\right)\exp\left(-j\frac{4\pi}{\lambda}R_0\right)$$

$$\cdot\operatorname{sinc}\left(B_a\left[t - \frac{x}{v_p} + \frac{x_e}{v_p}\right]\right)dxdy,\qquad(15)$$

where B_a and A_a denote the synthetic bandwidth and the pulse compression gain in azimuth, respectively.

It clearly shows that after two dimensional compressions, the point target has been well focused in the range-azimuth plane, only a minor shift determined by the relative position of the mth transmit and nth receive antenna is presented for each transmit-receive pair.

A co-registration operation is executed in range-Doppler domain, then

$$
\begin{aligned}
\tilde{y}_{mn}\left(\hat{t}, t\right) &= \mathcal{F}^- \left\{ y_{mn}(\hat{t}, t) \cdot \exp\left(-j2\pi f_a \frac{x_e}{v_p}\right) \right\} \\
&= \iint\limits_{x,y \in \Omega} \sigma_c\left(x, y\right) A_r A_a \operatorname{sinc}\left(B_r\left[\hat{t} - \frac{R_{mn}(t)}{c}\right]\right) \\
&\quad \cdot \exp\left(-j\frac{4\pi}{\lambda} R_0\right) \operatorname{sinc}\left(B_a\left[t - \frac{x}{v_p}\right]\right) dxdy, \quad (16)
\end{aligned}
$$

where $\mathcal{F}^-\left\{\cdot\right\}$ denotes the inverse Fourier transform.

It is interesting to note that the images obtained by different transmit-receive pairs are the same after sophisticated co-registration for stationary targets.

3.2. Imaging Processing for Moving Target

Similarly with the processing of the stationary target, azimuth compression is executed by the matched filter in (13), thereby the mnth complex image can be written as

$$
\begin{aligned}
I_{mn}\left(\hat{t}, t\right) &= \sum_{i=1}^{N_T} \sigma_{T,i}\left(x, y\right) A_r \operatorname{sinc}\left(B_r\left[\hat{t} - \frac{R_{mn}(t)}{c}\right]\right) \\
&\quad \cdot A_a \sin c\left(B_a\left[t - \frac{x}{v_p} + \frac{x_e}{v_p} + \frac{v_r R_0}{v_p^2}\right]\right) \\
&\quad \cdot \exp\left(-j\frac{2\pi}{\lambda}\left[2R_0 + 2x\frac{v_r}{v_p} - \left(\frac{v_r}{v_p}\right)^2 R_0\right]\right) \cdot \exp\left(j2\pi\frac{2v_r}{\lambda}\frac{x_e}{v_p}\right). \quad (17)
\end{aligned}
$$

Relatively to the image of the stationary target, there is an additional azimuth displacement $\Delta = v_r R_0/v_p$ due to the movement of target except for the Doppler shift resulting from the time delay between different transmit-receive pairs.

The operation of image co-registration is applied to remove the constant Doppler shift, therefore, multiple complex images can be

combined coherently to enhance the quality of the final image. The co-registration can be implemented in range-Doppler domain,

$$
\tilde{I}_{mn}\left(\hat{t}, t\right) = \mathcal{F}^- \left\{ I_{mn}(\hat{t}, t) \cdot \exp\left(-j2\pi f_a \frac{x_e}{v_p}\right)\right\}
$$

$$
= \sum_{i=1}^{N_T} \sigma_{T,i}\left(x, y\right) A_r A_a \operatorname{sinc}\left(B_r \left[\hat{t} - \frac{R_{mn}(t)}{c}\right]\right)
$$

$$
\cdot \operatorname{sinc}\left(B_a \left[t - \frac{x}{v_p} + \frac{v_r R_0}{v_p^2}\right]\right) \exp\left(j2\pi \frac{2v_r}{\lambda}\frac{x_e}{v_p}\right)
$$

$$
\cdot \exp\left(-j\frac{2\pi}{\lambda}\left[2R_0 + 2x\frac{v_r}{v_p} - \left(\frac{v_r}{v_p}\right)^2 R_0\right]\right). \qquad (18)
$$

For notational simplicity, we define

$$
\mathbf{a_T}(v_r) = \left[1, \exp\left(j\frac{2\pi v_r}{\lambda v_p}x_2^t\right), \ldots, \exp\left(j\frac{2\pi v_r}{\lambda v_p}x_M^t\right)\right]^{\mathrm{T}}, \qquad (19)
$$

$$
\mathbf{a_R}(v_r) = \left[1, \exp\left(j\frac{2\pi v_r}{\lambda v_p}x_2^r\right), \ldots, \exp\left(j\frac{2\pi v_r}{\lambda v_p}x_N^r\right)\right]^{\mathrm{T}}, \qquad (20)
$$

$$
A_I = \sum_T \sigma_t\left(x, y\right) A_r A_a \operatorname{sinc}\left(B_r \left[\hat{t} - \frac{R_{mn}(t)}{c}\right]\right)
$$

$$
\cdot \operatorname{sinc}\left(B_a\left[t - \frac{x}{v_p} + \frac{v_r R_0}{v_p^2}\right]\right) \cdot \exp\left(-j\frac{2\pi}{\lambda}\left[2R_0 + 2x\frac{v_r}{v_p} - \left(\frac{v_r}{v_p}\right)^2 R_0\right]\right). (21)
$$

Then the image can be denoted by

$$
\tilde{I}(\hat{t}, t) = A_I \odot \mathbf{a_T}\left(v_r\right) \otimes \mathbf{a_R}\left(v_r\right). \qquad (22)
$$

where $\otimes$ denotes Kronecker product, $\odot$ denotes Hadamard product, and $(\cdot)^{\mathrm{T}}$ denotes the transpose operation.

4. MOVING TARGET DETECTION AND VELOCITY ESTIMATION

The pixel vector of a moving target resulting from K equivalent virtual phase centers is denoted by

$$
S\left(t_i\right) = A_I \cdot \exp\left(j2\pi f_d t_i\right), \quad i = 1, 2, \ldots, K. \qquad (23)
$$

where $f_d = 2v_r/\lambda$ is the Doppler frequency, and $t_i = x_{e,i}/v_p$ is the equivalent spatial sampling time series.

Now, two important issues should be considered. First, we have to determine whether a moving target exists in a certain pixel vector. Second, the unknown velocity parameter should be accurately estimated for target relocation and imaging from the measurement data.

4.1. Moving Target Indication

A binary hypothesis testing problem, where a random vector $\mathbf{X}$ in $\mathbb{C}^K$, can be expressed as

$$
\begin{aligned}
H_0 &: \mathbf{X}(i) = \mathbf{C}(i) + \mathbf{N}(i), \quad i = 1, 2, \dots K \\
H_1 &: \mathbf{X}(i) = \mathbf{S}(i) + \mathbf{C}(i) + \mathbf{N}(i), \quad i = 1, 2, \dots K.
\end{aligned}
\tag{24}
$$

where $\mathbf{C}(i)$ denotes the clutter vector, which is modeled as complex Gaussian distribution with specified mean and covariance in [28], and $\mathbf{S}$ denotes the signal vector. The noise vector $\mathbf{N}$ is modeled as a realization of zero mean white complex Gaussian random process with a covariance matrix $\sigma_n^2 \mathbf{I}$, where σ_n^2 is the noise variance and $\mathbf{I}$ is an identity matrix.

The pixel vector is equivalent to conventional multi-channel SAR system with single transmitter and multiple receiver. Therefore, the detection and velocity estimation of the moving target can be directly obtained via "peak detection" in the Doppler spectrum by Fourier transform, which is similar to the conventional FFT-based VSAR processing [27, 28]. Nevertheless, FFT-based processing has its inherent limitations of low resolution and high sidelobe problems.

For the moving target detection in MIMO SAR image domain, the pixel vector to be detected is denoted by $\mathbf{X} = [x_1, x_2, \dots, x_K]^{\mathrm{T}}$, and an adaptive optimal weighted vector $\mathbf{w} = [w_1, w_2, \dots, w_K]^{\mathrm{T}}$ can be utilized to suppress the clutter. The complex output is given as

$$
y = \mathbf{w}_{\mathrm{opt}}^{\mathrm{H}} \mathbf{X}
\tag{25}
$$

where $(\cdot)^{\mathrm{H}}$ denotes the matrix Hermite operation.

The detailed derivation of the adaptive optimal weighting function can be found in significant literatures [28], which is given by

$$
\mathbf{w}_{\mathrm{opt}} = \mu \mathbf{R}^{-1} \mathbf{V}_{\mathrm{TR}}
\tag{26}
$$

where μ is a constant, $\mathbf{V}_{\mathrm{TR}} = \mathbf{a}_{\mathrm{T}} \otimes \mathbf{a}_{\mathrm{R}}$ is the joint transmit-receive steering vector, and the covariance matrix $\mathbf{R}$ is usually replaced by the sampling covariance matrix, which is estimated via L $(L > 2K)$ independent identically distributed (i, i, d) vector nearby the pixel to be detected. The maximum likelihood estimator may be given by

$$
\hat{\mathbf{R}} = \frac{1}{L} \sum_{l=1}^{L} \mathbf{X}_l \mathbf{X}_l^{\mathrm{H}}
\tag{27}
$$

Then the moving target detector is constructed by

$$\left| \mathbf{w}_{\text{opt}}^{\text{H}} \mathbf{X} \right| \underset{H_0}{\overset{H_1}{\gtrless}} \eta_0 \tag{28}$$

where η_0 is the threshold based on classical theory of detection, such as Constant False Alarm Ratio (CFAR) criterion.

4.2. Velocity Estimation

An alternative form of the pixel vector is expressed as

$$\mathbf{a}\left(\tilde{v}_r \right) = \begin{bmatrix} 1 \\ \tilde{\sigma} \cdot \exp\left(j \frac{2\pi}{\lambda} x_1^t \cdot \tilde{v}_r \right) \cdot \exp\left(j \frac{2\pi}{\lambda} x_1^r \cdot \tilde{v}_r \right) \\ \vdots \\ \tilde{\sigma} \cdot \exp\left(j \frac{2\pi}{\lambda} x_M^t \cdot \tilde{v}_r \right) \cdot \exp\left(j \frac{2\pi}{\lambda} x_N^r \cdot \tilde{v}_r \right) \end{bmatrix} \tag{29}$$

where $\tilde{v}_r = v_r / v_p$ is the normalized velocity.

We define

$$\mathbf{A} = \begin{bmatrix} \mathbf{a}_1 & \mathbf{a}_2 & \dots & \mathbf{a}_{N_T} \end{bmatrix}^{\text{T}}, \tag{30}$$

$$\mathbf{\Upsilon} = \begin{bmatrix} \Upsilon_1 & \Upsilon_2 & \dots & \Upsilon_{N_T} \end{bmatrix}^{\text{T}}, \tag{31}$$

where $\Upsilon_i = \sigma_i e^{j\phi_i}$, $(i = 1, 2, \dots, N_T)$ is the complex coefficient of the ith moving point scatter.

Without consideration of clutter signals, the pixel vector can be written by

$$\mathbf{z} = \mathbf{A}\mathbf{\Upsilon} + \mathbf{n}. \tag{32}$$

The problem of velocity estimation has been converted into a procedure for Direction of Arrival (DOA) estimation. For simplicity, the conventional DAS approach is applied for velocity estimation, thus,

$$\hat{v} = \arg\max \left| \mathbf{a}\left(\hat{v} \right) \mathbf{z} \right|. \tag{33}$$

5. SIMULATION EXAMPLES

Several simulation experiments will be done to illustrate the analysis aforementioned. For simplicity, we just consider a Uniform Linear Array (ULA) consisting of multiple transmitters and multiple receivers. A set of orthogonal phase coded waveforms is assumed in the following simulations. The other primary parameters of the SAR system and platform are listed in Table 1. It is important to note that the parameters in the following simulations are selected flexibly to show the results more clearly, it does not mean the parameters listed are feasible for practical system.

Table 1. Specification of simulated scene.

SAR System Parameters		Platform Parameters	
Transmit subaperture	3	Platform Altitude	4000 m
Receive subaperture	3	Slant Range	15 km
Subaperture length	2 m	Extent in Range	[−200 m 200 m]
Subaperture Interval	7.5 m	Velocity	110 m/s
Carrier Frequency	15.4 GHz	Extent in Azimuth	[−200 m 200 m]
Pulse Width	5 μs	PRF	2000 Hz
Bandwidth	150 MHz	-	-
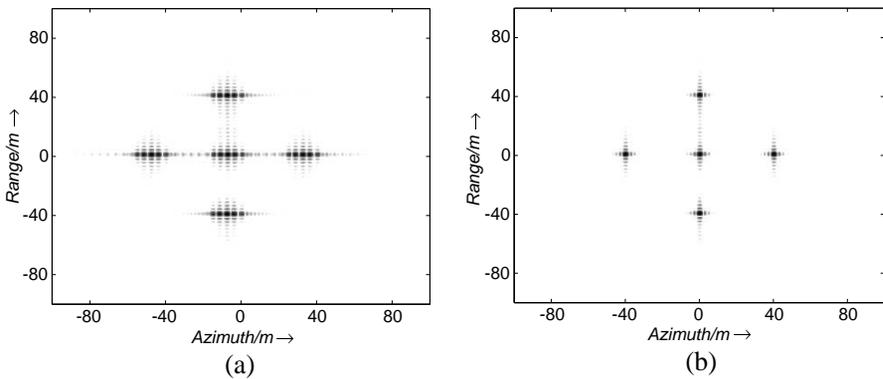
Figure 2. Point scatterers imaging results: (a) images integration without phase compensation; (b) coherent integration of multiple images.

5.1. Azimuth Displacement Compensation

There are a variety of schemes for combining the return from multiple transmit-receive pairs. An intuitive approach is to use the conventional range-Doppler (RD) algorithm for imaging based on the multi-channel data [13]. Five stationary point scatterers are assumed in the scene, and the imaging result without phase compensation is shown in Fig. 2(a), which clearly indicates that there is an azimuth displacement between any two images formed by different transmit-receive pairs due to the spatial phase differences. The displacement can be removed via phase compensation in range-Doppler domain for each transmit-receive pair, the ultimate composite image is shown in Fig. 2(b).

To verify the signal model and the effect of azimuth displacement due to the displacement of the equivalent phase centers more

realistically, a simulated raw data of stationary scene based on the grey level of a well focused SAR image is reconstructed by the algorithms in [29]. Fig. 3(a) shows the composite SAR image which is affected by uncompensated spatial phase differences between different transmit-receive pairs. In contrast, the compensated image of MIMO SAR is shown in Fig. 3(b).

5.2. Performance Comparison versus Different Array Configuration

A number of studies have proven the advantages that MIMO radar could obtain at most MN independent images via M transmit


(a)   (b)
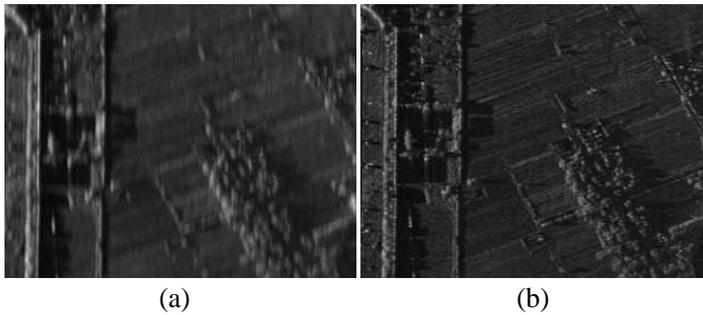
Figure 3. Scene simulation results: (a) composite image without phase compensation; (b) composite image after phase compensation.

(a)   (b)

(c)   (d)
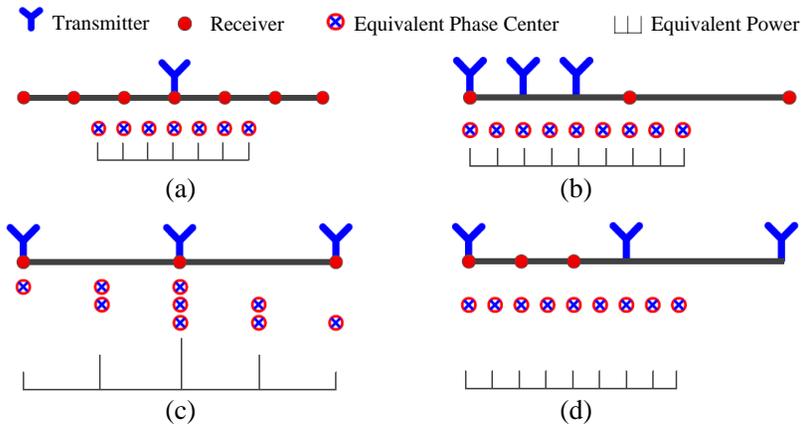
Figure 4. MIMO SAR array configuration. (a) SIMO SAR; (b) full array transmit and sparse array receive; (c) MIMO community antennas; (d) sparse array transmit and full array receive.

antennas and N receive antennas. For conciseness, several typical configuration of transmit-receive linear arrays are shown in Fig. 4. Two important advantages are shown in Fig. 4. Firstly, the MIMO SAR system could achieve much more equivalent phase centers than the Single-Input Multi-Output (SIMO) configuration with equal number of practical transmit and receive antennas, which means that compared with traditional multi-channel SAR systems, SAR based on MIMO configuration provides a low cost strategy; Secondly, the equivalent full array can be formed by sparse array configuration, which means that we could make use of the benefit of sparse array without the the effect of gratelobe.

The performance of clutter suppression by different array
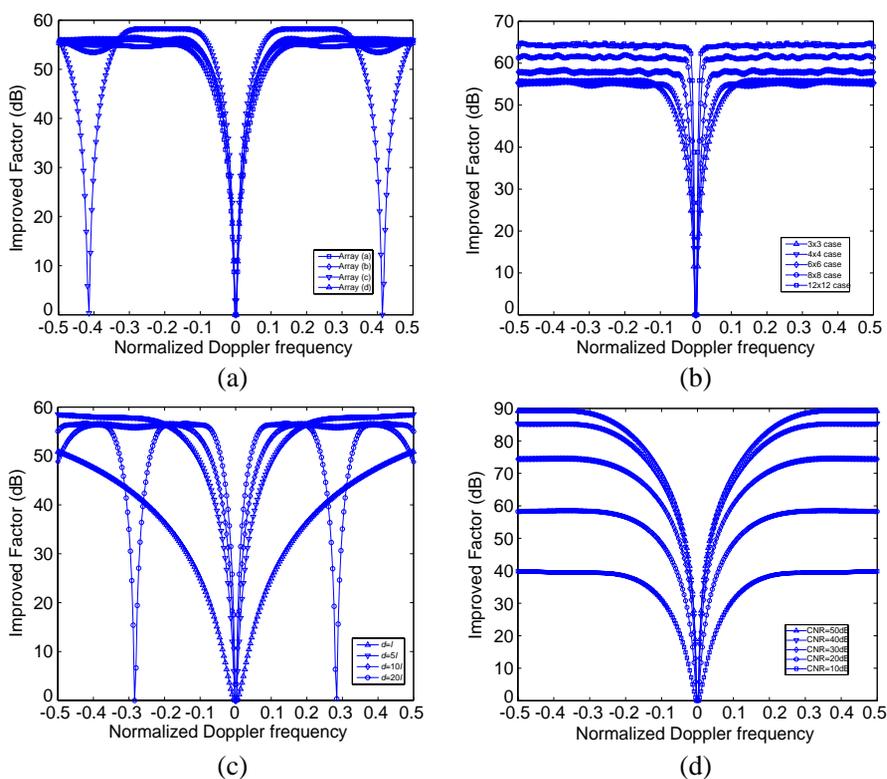
Figure 5. IF versus normalized Doppler with different parameters. (a) IF variation with variety of array configuration; (b) IF variation with the number of transmit-receive antennas; (c) IF variation with different antenna spacings; (d) IF variation with different CNR.

configuration is validated here. The Improvement Factor (IF), which is defined as the output Signal-to-Clutter-Noise Ratio (SCNR) to the input SCNR [31], is given by

$$\text{IF} = \mathbf{V}_{\text{TR}}^{\text{H}} \mathbf{R}^{-} \mathbf{V}_{\text{TR}} \frac{\text{tr}\,(\mathbf{R})}{\mathbf{V}_{\text{TR}}^{\text{H}} \mathbf{V}_{\text{TR}}} \qquad (34)$$

The comparison results are shown in Fig. 5. The result in Fig. 5(a) shows that the improvement factor is dependent upon the array manifold of the equivalent virtual array. Therefore, with reasonable placement of the multiple transmit and receive antennas, a large equivalent aperture can be achieved by fewer practical antennas. Fig. 5(b) indicates that the improvement factor is a monotonically increasing function of the number of the equivalent phase centers. Nevertheless, the number of transmit and receive antenna is limited by a variety of factors, such as load, volume, and power of the platform. A typical three-transmit and three-receive MIMO SAR system with different antenna spacing is shown in Fig. 5(c), which confirms the conclusion that MIMO array make use of the benefit of sparse array without the the effect of gratelobe. The result in Fig. 5(d) shows that the larger the Clutter-to-Noise Ratio (CNR) of the original pixel, the better detection performance could be obtained. Compared to conventional approach for clutter suppression in complex data domain, the primary compressions both in range and azimuth direction have improved the CNR significantly, therefore, the higher IF may be obtained for MIMO SAR system.
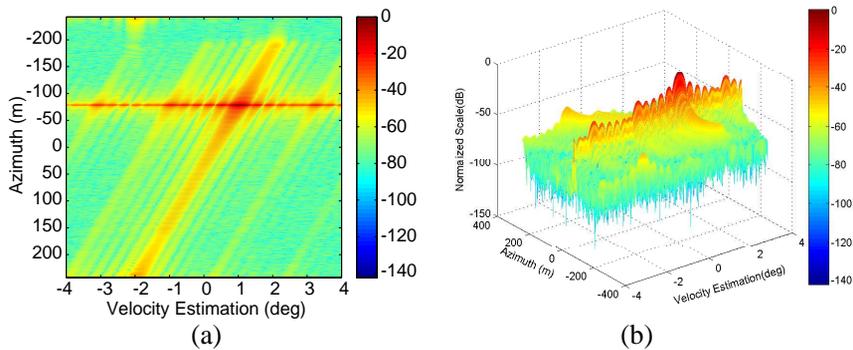
Figure 6. Velocity estimation results: (a) 2-D plot version; (b) 3-D plot version.

5.3. Velocity Estimation

We assume that a moving target is located at the center of the imaging scene with an azimuth angle $\theta = 0.113°$. The speed of the moving target is assumed to be $1.0\,\text{m/s}$, and the angle between the moving direction and the light of sight is $\varphi = 135°$. The result of velocity estimation is shown in Fig. 6(a), and a 3-D version is shown in Fig. 6(b). It shows that the DAS suffers from high sidelobe level and low resolution, which may cause false detection and poor velocity estimation. Fortunately, a wide range of alternative spectral estimation techniques, such as Capon, APES, MUSIC, GLRT, and the recently proposed IAA algorithm [32], are available to perform this operation.

6. CONCLUSION

In this paper, we have presented an end-to-end signal model of MIMO SAR both for stationary and ground moving targets, and the approaches for target detection and parameter estimation based on multi-channel SAR images are then discussed. This study has confirmed the advantage that more equivalent virtual phase centers could be achieved via multi-input multi-output conception, which indicates the potential ability to resolve the inherent contradicting requirements for high resolution wide-swath imaging. Furthermore, the larger virtual aperture and higher DOF provide an avenue to adaptively suppress the mainlobe clutter and interferences.

In this paper, we mainly focus on the presentation of the signal model and the analysis of motion effect based on the newly emerged MIMO SAR concept. However, the derivation and analyses should be regarded as a first step for MIMO SAR systems, further studies on the approaches for adaptive clutter suppression and parameter estimation will be summarized in the further work.

ACKNOWLEDGMENT

REFERENCES

1. Li, J. and P. Stoica, "MIMO radar with colocated antennas," *IEEE Signal Processing Magazine*, Vol. 24, No. 5, 106–114, 2007.

2. Haimovich, A. M., S. Blum, and L. J. Cimini, "MIMO radar with widely separated antennas," *IEEE Signal Processing Magazine*, Vol. 25, No. 1, 116–129, 2008.

3. Qu, Y., G. Liao, S.-Q. Zhu, X.-Y. Liu, and H. Jiang, "Performance analysis of beamforming for MIMO radar," *Progress In Electromagnetics Research*, Vol. 84, 123–134, 2008.

4. Lim, S. H., "Shifting MIMO SAR system for high-resolution wide-swath imaging," *Journal of Electromagnetic Waves and Applications*, Vol. 25, Nos. 8–9, 1168–1178, 2011.

5. Chen, H.-W., X. Li, J. Yang, W. Zhou, and Z. Zhuang, "Effects of geometry configurations on ambiguity properties for bistatic MIMO radar," *Progress In Electromagnetics Research B*, Vol. 30, 117–133, 2011.

6. Hatam, M., A. Sheikhi, and M. A. Masnadi-Shirazi, "Target detection in pulse-train MIMO radars applying ICA algorithms," *Progress In Electromagnetics Research*, Vol. 122, 413–435, 2012.

7. Chen, J., Z. Li, and C. S. Li, "A novel strategy for topside ionosphere sounder based on spaceborne MIMO radar with FDCD," *Progress In Electromagnetics Research*, Vol. 116, 381–393, 2011.

8. Krieger, G., N. Gebert, and A. Moreira, "Multidimensional waveform encoding: A new digital beamforming technique for synthetic aperture radar remote sensing," *IEEE Transactions on Geoscience and Remote Sensing*, Vol. 46, No. 1, 31–46, 2008.

9. Li, J., S. S. Zhang, and J. F. Chang, "Applications of compressed sensing for multiple transmitters multiple azimuth beams SAR imaging," *Progress In Electromagnetics Research*, Vol. 127, 259–275, 2012.

10. Das, A., R. Cobb, and M. Stallard, "TechSat 21: A revolutionary concept in distributed space based sensing," *AIAA Defense and Civil Space Programs Conference and Exhibit.*, 28–30, Huntsville, AL, 1998

11. Xu, W., P. Huang, and Y.-K. Deng, "Multi-channel SPCMB-tops SAR for high-resolution wide-swath imaging," *Progress In Electromagnetics Research*, Vol. 116, 533–551, 2011.

12. Xu, W., P. P. Huang, and Y. K. Deng, "MIMO-tops mode for high-resolution ultra-wide-swath full polarimetric imaging," *Progress In Electromagnetics Research*, Vol. 121, 19–37, 2011.

13. Zhou, W., H. W. Chen, K. L. Li, and X. Li, "A novel algorithm for MIMO SAR imaging," *Journal of Electromagnetic Waves and Applications*, Vol. 26, No. 8, 1082–1094, 2012.

14. Wang, W. Q., "Space-time coding MIMO-OFDM SAR for high-resolution imaging," *IEEE Transactions on Geoscience and Remote Sensing*, Vol. 49, No. 8, 3094–3104, 2011.

15. Ender, J., "MIMO-SAR," *IEEE International Geoscience and Remote Sensing Symposium*, 5310–5314, 2007.

16. Cristallini, D. and D. Pastina, "Exploiting MIMO SAR potentialities with efficient cross-track constellation configurations for improved range resolution," *IEEE Transactions on Geoscience and Remote Sensing*, Vol. 49, No. 1, 38–52, 2010.

17. Kim, J., "Investigation of MIMO SAR for interferometry," *Proceedings of the 4th European Radar Conference*, 51–54, 2007.

18. Friedlander, B., "MIMO-VSAR: A high resolution radar system for imaging moving scenes," *The 44th Asilomar Conference on Signals Systems and Computer*, 2143–2147, 2010.

19. Dai, X. Z., J. Xu, Y. N. Peng, and Y. L. Wang, "MIMO-VSAR and a kind of optimized array configuration," *Acta Electronica Sinica*, Vol. 36, No. 12, 2394–2399, 2008.

20. Brenner, A. R. and J. Ender, "Demonstration of advanced reconnaissance techniques with the airborne SAR/GMTI sensor PAMIR," *IEE Proceeding — Radar, Sonar and Navigation*, Vol. 153, No. 2, 152–162, 2006.

21. Klare, J., "MIRA-CLE X: A new imaging MIMO-radar for multi-purpose applications," *Proceedings of the 7th European Radar Conference*, 2010.

22. Kantor, J. and S. K.Davis, *Airborne GMTI Using MIMO Techniques*, MIT Lincoln Laboratory, Lexington, MA, Tech. Rep. TR-1150, 2011.

23. Li, S. F., J. Chen, L. Q. Zhang, and Y. Q.Zhou, "Complete complementary sequence for MIMO SAR," *Progress In Electromagnetics Research C*, Vol. 13, 51–66, 2010.

24. Huang, Y. and P. V. Brennan, "FMCW based MIMO imaging radar for maritime navigaiton," *Progress In Electromagnetics Research*, Vol. 115, 327–342, 2011.

25. Roberts, W., H. He, J. Li, and P. Stoica, "Probing waveform synthesis and receiver filters design," *IEEE Signal Processing Magazine*, Vol. 27, No. 4, 99–112, 2010.

26. Cumming, I. G. and F. H. Wong, *Digital Processing of Synthetic Aperture Radar Data: Algorithms and Implementation,* Artech

House, 2005.

27. Friedlander, B. and B. Porat, "VSAR: A high-resolution radar system for a high resolution radar system for detection of moving targets," *IET Radar Sonar and Navigation*, Vol. 144, No. 4, 205–218, 1997.

28. Xu, J., G. Li, Y. N. Peng, X. G. Xia, and Y. L. Wang, "Parametric velocity synthetic aperture radar: Signal modeling and optimal methods," *IEEE Transactions on Geoscience and Remote Sensing*, Vol. 46, No. 9, 2463–2480, 2010.

29. Franceschetti, G., A. Iodice, S. Perna, and D. Riccio, "Efficient simulation of airborne SAR raw data of extended scenes," *IEEE Transactions on Geoscience and Remote Sensing*, Vol. 44, No. 10, 2851–2860, 2006.

30. Chan, Y. K. and V. C. Koo, "An introduction to synthetic aperture radar (SAR)," *Progress In Electromagnetics Research B*, Vol. 2, 27–60, 2008.

31. Klemm, R., *Principles of Space-time Adaptive Processing,* 3rd Edition, IET Radar, Sonar, Navigation and Avionics Series 21, 2006.

32. Yardibi, T., J. Li, P. Stoica, M. Xue, and A. B. Baggeroer, "Source localization and sensing: A nonparametric iterative adaptive approach based on weighted least squares," *IEEE Transactions on Aerospace and Electronic Systems*, Vol. 46, 425–443, 2010.